American Mineralogist, Volume 104, pages 996–1004, 2019

A low-aluminum clinopyroxene-liquid geothermometer for high-silica magmatic systems

Karalee K. Brugman[1,*] and Christy B. Till[1]

[1]School of Earth and Space Exploration, Arizona State University, Tempe, Arizona 85287, U.S.A.

Abstract

Several geothermobarometric tools have focused on clinopyroxene due to its prevalence in igneous rocks, however clinopyroxene produced in high-silica igneous systems is high in iron and low in aluminum, causing existing geothermometers that depend on aluminum exchange to fail or yield overestimated temperatures. Here we present a new clinopyroxene-liquid geothermometer recommended for use in natural igneous systems with bulk $SiO_2 \geq 70$ wt%, which contain clinopyroxene with Mg# ≤ 65 and $Al_2O_3 \leq 7$ wt%.

$$T(°C) = 300\left[\begin{array}{l} -1.89 - 0.601\left(X^{Cpx}_{CaTs}\right) - 0.186\left(X^{Cpx}_{DiHd_{2003}}\right) + 4.71\left(X^{liq}_{SiO_2}\right) + 77.6\left(X^{liq}_{TiO_2}\right) \\ +10.9\left(X^{liq}_{FeO}\right) + 33.6\left(X^{liq}_{MgO}\right) + 15.5\left(X^{liq}_{CaO}\right) + 15.6\left(X^{liq}_{KO_{0.5}}\right) \end{array}\right] \quad (1)$$

The new geothermometer lowers calculated temperatures by ~85 °C on average relative to Putirka (2008, Eq. 33) and reduces the uncertainty by a factor of two (standard error of estimate ±20 °C). When applied to natural systems, we find this new clinopyroxene-liquid geothermometer reconciles many inconsistencies between experimental phase equilibria and preexisting geothermometry results for silicic volcanism, including those from the Bishop Tuff and Yellowstone caldera-forming and post-caldera rhyolites. We also demonstrate that clinopyroxene is not restricted to near-liquidus temperatures in rhyolitic systems; clinopyroxene can be stable over a broad temperature range, often down to the solidus. An Excel spreadsheet and Python notebook for calculating temperature with this new geothermometer may be downloaded from GitHub at http://bit.ly/cpxrhyotherm.

Keywords: Geothermometer, clinopyroxene, high-silica

Introduction

Investigations of igneous systems often begin with an assessment of the temperature during eruption, crystallization, and/or magma storage, and geothermometers are generally calibrated to work with a broad range of rock types and mineral compositions. At least 40 clinopyroxene geothermometers have been developed, and many improve on past geothermometers or build on a previously published activity model. Two-pyroxene geothermometers are the most common type (e.g., Lindsley and Andersen 1983; Anderson et al. 1993; Sack and Ghiorso 1994; Putirka 2008; Liang et al. 2013) and take advantage of the temperature-dependent solvus of the pyroxene system. But these geothermometers necessitate the presence of equilibrium pairs of clinopyroxene and orthopyroxene in the host rock and are almost exclusively calibrated for diopside (Di; $CaMgSi_2O_6$), the low-Fe end-member of calcic clinopyroxene. Another type of geothermometer, clinopyroxene-liquid (e.g., Putirka 2008; Masotta et al. 2013), does not require co-crystallizing orthopyroxene and relies on the equilibria of Di, hedenbergite (Hd; $CaFeSi_2O_6$), and jadeite (Jd; $NaAlSi_2O_6$), the high-Al end-member of sodic clinopyroxene. However, geothermometers dependent on this equilibria are likely to be inaccurate if there is very little Al in the clinopyroxene and thus very little to no Jd component (which is calculated based on the estimated Al^{IV} rather than Na when Al^{IV} is low—see Supplemental[1] Table S1). This caveat becomes significant when studying high-silica systems in which clinopyroxene is typically high in Fe (up to 30 wt% oxide) and low in Al (<2 wt% oxide; Fig. 1).

Unfortunately, the high-Fe, low-Al clinopyroxene from high-silica systems are not well represented in experimental data used to calibrate existing geothermometers, as the majority of experimental studies tend to explore Mg-rich augite to diopside, and in mafic rather than silicic systems. In silica-saturated systems, the major phases are Al-bearing plagioclase and alkali feldspar, and clinopyroxene have relatively low CaO; consequently, these clinopyroxene crystallize with almost all tetrahedral sites filled with Si rather than Al (Salviulo et al. 2000). A result of the historical sampling bias is that in Al_2O_3-Mg# space, there is no overlap between the clinopyroxene found in many natural high-silica magmatic systems and the clinopyroxene used to calibrate two of the most commonly used clinopyroxene geothermometers, the Putirka (2008) clinopyroxene-liquid geothermometer and the MELTS two-pyroxene geothermometer (Sack and Ghiorso 1994) (Fig. 1). For many high-Fe, low-Al clinopyroxene, the most popular clinopyroxene-liquid geothermometer (Putirka 2008, Eq. 33) does not successfully calculate a temperature. When it does, it returns systematically high temperatures, up to 170 °C greater than the conditions of high-Fe, low-Al clinopyroxene-saturated

* E-mail: kara.brugman@asu.edu

0003-004X/19/0007–996$05.00/DOI: https://doi.org/10.2138/am-2019-6842

experiments, indicating that this geothermometer is not well suited for this restricted mineral composition. Thus, if we wish to utilize clinopyroxene in our thermal investigations of high-silica systems such as Long Valley, Yellowstone, and Valles Calderas, it is prudent to develop a new geothermometer that is calibrated for the clinopyroxene found in these eruptive products.

Here we present a new clinopyroxene-liquid geothermometer, calibrated using data from experiments on high-silica systems that crystallized high-Fe, low-Al clinopyroxene, that is able to consistently calculate temperatures where other geothermometers fail and reproduce experimental temperatures to within 17 °C. Also, for high-silica system experiments below 850 °C—the temperature range of most interest for these systems—the new clinopyroxene-liquid geothermometer offers a fivefold decrease in the deviation between calculated and actual experimental temperatures as compared to the Putirka (2008, Eq. 33) geothermometer (±20 vs. ±110 °C). We apply the geothermometer to a series of silicic igneous systems to examine the effect of these adjusted temperatures on our petrologic understanding of phase relations and magma storage conditions.

Methods

To calibrate a new geothermometer, a data set of clinopyroxene and glass compositions was compiled from recent experimental studies on high-silica magmatic systems (Supplemental[1] Table S2). The selected studies were conducted at 675–1025 °C and 75–503 MPa and yielded experimental run products with a bulk silica content of >70 wt% and clinopyroxene with ≤7 wt% Al_2O_3 and Mg# from 2.5–77 (Fig. 1, Supplemental[1] Table S2). These data included relatively few experiments performed between 750–875 °C, therefore new hydrothermal cold-seal pressure vessel (CSPV) experiments (4) were conducted in this temperature range to supplement the experiments from the literature.

For the new experiments, the starting material, the Scaup Lake rhyolite from Yellowstone Caldera (sample 12CTYC-01), was twice powdered, homogenized, and glassed at 1400 °C for 30 min in a 1 atm vertical furnace at the Experimental Petrology and Igneous Processes Center (EPIC) at Arizona State University (ASU) (Table 1). Single Scaup Lake clinopyroxene crystals with intact, euhedral faces were hand-picked under stereo microscope from a ≤1 mm size fraction of mineral separates to mitigate compositional heterogeneity due to subtle intracrystalline zoning. These clinopyroxene were used as seed crystals in the whole-rock powder. The CSPV experiments were conducted at the Massachusetts Institute of Technology experimental petrology lab in Stellite No. 25 cold-seal hydrothermal pressure vessels with filler rods, and were heated in horizontal, split-tube furnaces. Temperatures were monitored using chromel-alumel thermocouples. Experiments were H_2O-saturated and buffered at NNO using double Au capsules with powdered Ni-NiO buffer in the outer capsule. The pressure for all experiments was 1 kbar, run durations were ~16–24 days (Table 2), and experiments were quenched by blowing compressed air over the vessels while at pressure. After quenching, inner and outer capsules were weighed before and after they were pierced and dried in a warming oven for 10 min. If mass was lost after piercing and drying, often in conjunction with water visible upon piercing, the capsule was presumed to be H_2O-saturated.

The CSPV experimental products (Supplemental[1] Table S2) were mounted in epoxy in wells drilled into 1″ aluminum rounds and then measured on the JXA-8530F EPMA at ASU's Eyring Materials Center using an accelerating voltage of 15 kV and beam current of 15 nA. Beam sizes were 1 μm for clinopyroxene and 10 μm for glass. Time-dependent intensity (TDI) correction was applied to glass measurements of Na, K, and Si to mitigate migration of light elements away from the electron beam.

Results

CSPV calibration experiments

Four successful experiments (750–825 °C, 1 kbar) were glassy with bubbles and included amphibole, indicating the charges remained H_2O-saturated for the run duration. All experiments crystallized clinopyroxene (Fig. 2, Supplemental[1] Table S2) and contained equilibrated, unzoned seed crystals, with variable minor amounts of alkali feldspar, plagioclase, Fe-Ti oxides, and quartz.

Accepted clinopyroxene data were sourced from crystals that showed no zoning in backscattered electron (BSE) images. These data were from either newly grown crystals or rims of equilibrated seed crystals (easily distinguished by size: < 50 μm

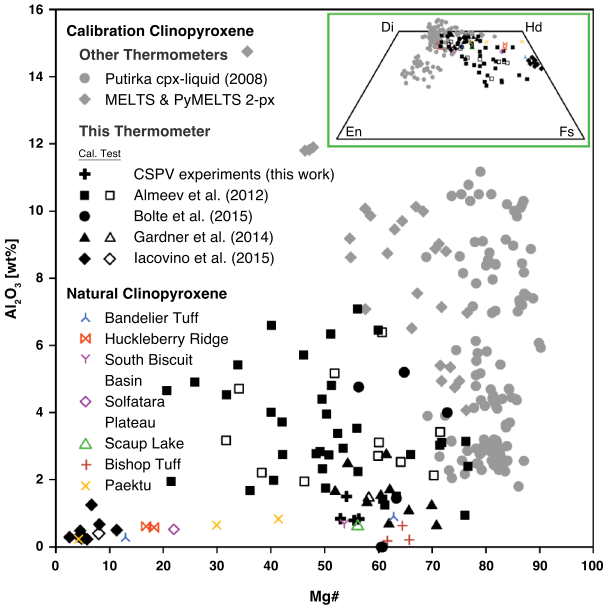

Figure 1. Clinopyroxene compositions from experiments and silicic igneous systems. Gray symbols: clinopyroxene used to calibrate existing geothermometers (Sack and Ghiorso 1994; Putirka, personal communication). Black solid and matching black outlined symbols: clinopyroxene used to calibrate and test the new clinopyroxene-liquid geothermometer (Almeev et al. 2012; Gardner et al. 2014; Bolte et al. 2015; Iacovino et al. 2015). Colored symbols: compositions of clinopyroxene from natural high-silica magmatic systems (Hildreth 1977; Warshaw and Smith 1988; Sisson 1991; Girard and Stix 2009; Gardner et al. 2014; Iacovino et al. 2016). Inset: Pyroxene quadrilateral of the same clinopyroxene as the main figure. (Color online.)

Table 1. Experiment starting glass

Oxide	wt%	St.dev.
SiO_2	74.59	2.73
TiO_2	0.23	0.15
Al_2O_3	13.75	1.96
Cr_2O_3	0.01	0.01
FeO^{tot}	1.75	0.71
MnO	0.04	0.03
MgO	0.19	0.09
CaO	1.03	0.34
Na_2O	2.55	0.37
K_2O	5.15	0.19

Note: EPMA data; n = 14.

Table 2. CSPV experimental conditions

Experiment	*T* (°C)	*P* (kbar)	*t* (h)
SCL01-4	750	1.0	573
SCL01-3	775	1.0	572
SCL01-5	800	1.0	385
SCL01-1	825	1.0	410

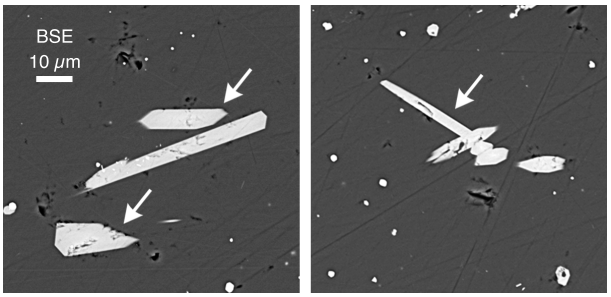

FIGURE 2. Clinopyroxene crystallized during CSPV experiment SCL01-3 (775 °C, 1 kbar, 572 h). Crystals used for calibration indicated with white arrows. Gray background is glass.

vs. ≥100 μm) that differed from their starting composition (Supplemental[1] Table S3).

Geothermometer calibration and performance

The CSPV experiment data were combined with the previously published experimental data. Sixty-four of these data points constitute the geothermometer calibration data set of high-Fe, low-Al clinopyroxene and glass pairs (Table 3, Supplemental[1] Table S2). Thirteen data points were not included in the calibration data set and instead were set aside as a test data set to check the efficacy of the geothermometer. To preserve temperature variation in the calibration data, a data point was excluded from the calibration data set and reserved for the test data set only if the experiment was conducted at the same temperature as other experiments in that particular study.

The calibration data set clinopyroxene and glass compositions (60 previously published and 4 from this work) were converted to clinopyroxene components and liquid cation fractions following the procedure used in previous clinopyroxene-liquid geothermometers (Putirka et al. 2003 and references therein) (see Supplemental[1] Table S1 for the full procedure). Backward step-wise regression was used to determine which parameters best explained the variation in experimental temperatures. Significant parameters were selected based on statistics of significance from preliminary linear regressions on the calibration data set. These initial linear regressions were performed with *T* as the dependent variable, and one of two groups of parameters as independent variables. Parameter Group A was comprised of those calculated for use in the Putirka (2008, Eq. 33) geothermometer and Group B encompassed Group A as well as calculations of cations based on 6 O atoms for clinopyroxene (Supplemental[1] Table S1). A parameter progressed to the next stage of the process if the 95% confidence interval for its coefficient did not include 0.

These limited sets of parameters were used in new linear regression trials to create new candidate geothermometer equations. These equations were evaluated for efficacy by their ability to return accurate temperatures from the test data set [e.g., R^2 and standard error of estimate (SEE)]. Ultimately, the parameters from both clinopyroxene and liquid that most improved regression statistics were sourced from Group A, resulting in the geothermometer equation:

$$T(°\mathrm{C}) = 300\begin{bmatrix} -1.89 - 0.601\left(X^{\mathrm{Cpx}}_{\mathrm{CaTs}}\right) - 0.186\left(X^{\mathrm{Cpx}}_{\mathrm{DiHd}_{2003}}\right) + 4.71\left(X^{\mathrm{liq}}_{\mathrm{SiO_2}}\right) + 77.6\left(X^{\mathrm{liq}}_{\mathrm{TiO_2}}\right) \\ +10.9\left(X^{\mathrm{liq}}_{\mathrm{FeO}}\right) + 33.6\left(X^{\mathrm{liq}}_{\mathrm{MgO}}\right) + 15.5\left(X^{\mathrm{liq}}_{\mathrm{CaO}}\right) + 15.6\left(X^{\mathrm{liq}}_{\mathrm{KO_{0.5}}}\right) \end{bmatrix} \quad (1)$$

$X^{\mathrm{Cpx}}_{\mathrm{DiHd}_{2003}}$ represents the Di plus Hd components of clinopyroxene as described in Putirka et al. (2003), and $X^{\mathrm{liq}}_{\mathrm{SiO_2}}$ represents the cation fraction of SiO_2 in the liquid.

The new geothermometer reproduced the temperatures of the test data set well, with an R^2 value of 0.95 as compared to R^2 = 0.72 for temperatures calculated using the Putirka (2008) clinopyroxene-liquid geothermometer (using Putirka 2008 Eq. 33 in concert with the reported experimental *P*) (Fig. 3b). Based on results from the test data set, the new geothermometer has a SEE of ±20 °C, and when applied to both the calibration and test data sets of high-Fe, low-Al experimental clinopyroxene, recovers these temperatures to within an average of 17 °C. In comparison, the Putirka (2008, Eq. 33) geothermometer, which is calibrated for a broad range of systems, has a reported SEE of ±45 °C, and can overestimate the same experiments' temperatures by >170 °C. For experiments performed ≤850 °C, the new geothermometer returned temperatures within an average of 20 °C, a fivefold improvement over the Putirka (2008, Eq. 33) clinopyroxene-liquid geothermometer (Fig. 3).

The new geothermometer eliminates any dependence on Jd, and the H_2O and pressure terms in the Putirka (2008, Eq. 33) geothermometer were found to have no significant effect on this empirical calibration. The only clinopyroxene parameters on which the geothermometer relies are the Ca-Tschermak's (CaTs) and $DiHd_{2003}$ components. The new geothermometer has a strong dependence on the TiO_2 and MgO content of the liquid, and greatly increases the dependence on SiO_2 and CaO in the liquid over that of the Putirka (2008, Eq. 33) geothermometer. Because of the new geothermometer's strong dependence on the liquid composition, for input conditions we recommend only using actual glass compositions measured as close as is prudent to the clinopyroxene of interest. This is in part because the rhyolitic whole rock oxide composition can deviate from that of the glass, particularly in those oxides used in the geothermometer, e.g., MgO, that tend to be higher in crystal cores. Using whole rock instead of glass compositions with the geothermometer increases the SEE of the calculated temperature. For example, a temperature calculated for Bishop Tuff samples using whole rock is >60 °C higher (>3× the SEE) than a temperature calculated correctly with glass.

Calibration trials were also conducted using the same parameters as the Putirka (2008, Eq. 33) clinopyroxene-liquid geothermometer, including Jd and *P*. Although temperature estimates using these parameters were somewhat improved over the original Putirka (2008, Eq. 33) geothermometer (SEE ± 30 vs. ± 60 °C for our test data set), this parameterization produced a lower R^2 than our new empirically based regression equation (0.81 vs. 0.95) and the SEE was ~10 °C greater (SEE ± 30 vs. ± 20 °C) for both the entire test data set and the experiments performed ≤850 °C.

TABLE 3. Calibration data set experimental conditions

Locality	*n*	*T* (°C)	*P* (kbar)
Scaup Lake rhyolite	4	750–825	1.0
Cougar Point and Indian Batt rhyolites[a]	36	875–1025	2.0–5.03
Blacktail Creek rhyolite tuff[b]	4	790–850	2.0
Late-erupted Bishop Tuff pumice[c]	10	700–800	1.0–2.0
Paektu Millennium comendite pumice[d]	10	675–750	0.5–1.5

Notes: Composition data from [a] Almeev et al. (2012), [b] Bolte et al. (2015), [c] Gardner et al. (2014), and [d] Iacovino et al. (2015) are available in Supplemental[1] Table S2.

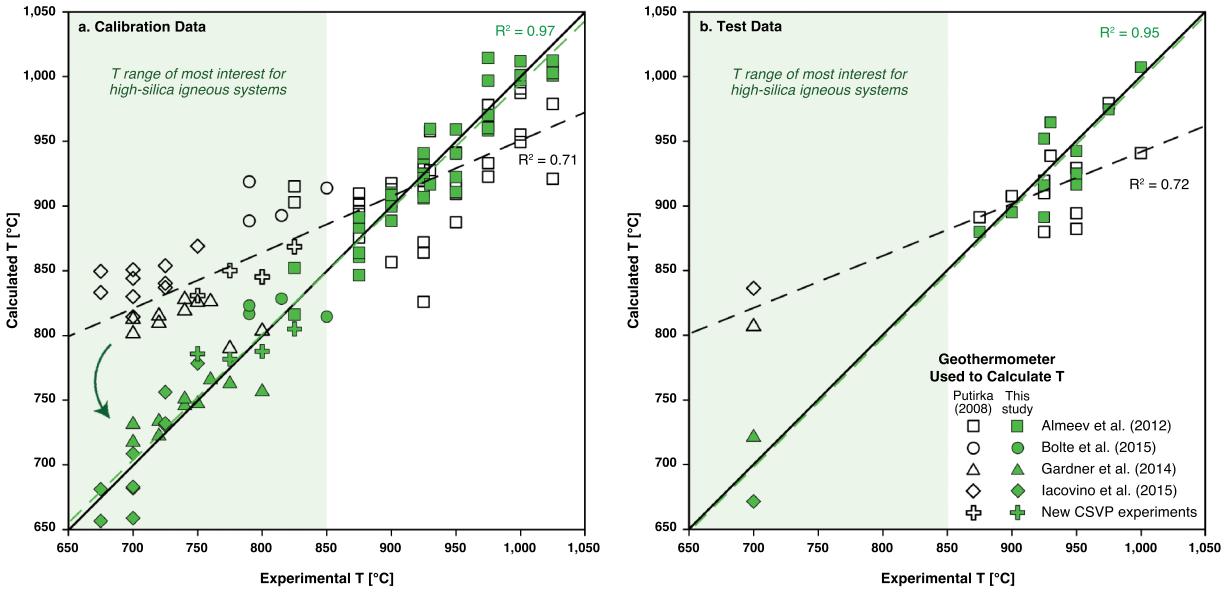

FIGURE 3. Calculated vs. experimental temperature. Temperatures are calculated using both the Putirka (2008, Eq. 33) clinopyroxene-liquid geothermometer (open symbols) and the new geothermometer (solid green symbols), and are plotted against the experimental conditions. Symbols are the same for both panels. The solid line represents unity between the calculated and experimental temperatures. Dashed lines show the best fit through each data set to better illustrate the new geothermometer's efficacy. (**a**) Calibration data. Arrow emphasizes that in the temperature range of most interest for high-silica magmatic systems, temperatures calculated with the new geothermometer are consistently closer to unity. (**b**) Test data. (Color online.)

This result is not surprising, because although the Putirka (2008) geothermometer is thermodynamically motivated, it relies on Di, Hd, and Jd equilibria. The Jd content of natural high-silica system clinopyroxene can be zero, and the estimated Jd content of the new geothermometer's calibration data set is as low as 0.002.

Additionally, we explored a universal clinopyroxene-liquid geothermometer calibrated with a data set comprised of both our calibration data set and that used to calibrate Putirka (2008, Eq. 33). Although this geothermometer was able to return a temperature for all test data and improved SEE of experiments conducted ≤850 °C vs. the original Putirka (2008, Eq. 33) geothermometer, it was not pursued as it did not improve the SEE for the high-Fe, low-Al test or calibration data sets. And, with $R^2 = 0.80$, the universal geothermometer had the poorest R^2 value of any of the candidate geothermometer equations. This is also not surprising, as the two calibration data sets—our high-Fe, low-Al clinopyroxene and Putirka (2008)'s generally more mafic clinopyroxene—have little overlap in Al_2O_3 vs. Mg# space or on the pyroxene quadrilateral (Fig. 1).

Although the Putirka (2008, Eq. 33) clinopyroxene-liquid geothermometer was calibrated to be broadly applied and is an excellent tool for use with the majority of igneous rock compositions, including more augitic or high-Al clinopyroxene from high-silica systems, high-Fe, low-Al clinopyroxene appear to be an end-member case that requires special handling. For high-Fe, low-Al clinopyroxene, a universal geothermometer is unable to match the accuracy of a specialized tool.

In some cases, the temperatures calculated with the new geothermometer are within the uncertainty of the Putirka (2008, Eq. 33) geothermometer. However, the Putirka (2008) geothermometer will sometimes fail to return a temperature for high-Fe, low-Al clinopyroxene, particularly if Jd = 0 (i.e., when $Al^{IV} = 0$), and the new geothermometer eliminates this issue in addition to decreasing uncertainty. Although the new geothermometer calibration data set clinopyroxene has median 2.25 wt% Al_2O_3 (23% of the data set has <1 wt%) it includes clinopyroxene with up to 7.08 wt% Al_2O_3 (Fig. 1). Thus, our new clinopyroxene-liquid geothermometer is recommended for use with natural systems that have bulk $SiO_2 \geq 70$ wt% and bear clinopyroxene with Mg# ≤ 65 and $Al_2O_3 \leq 7$ wt%. An Excel spreadsheet and Python notebook for calculating temperature with this new geothermometer are included in the Supplemental Materials[1]. The most up to date version may be downloaded from GitHub at http://bit.ly/cpxrhyotherm.

Equilibrium of natural samples

An important question when considering using a clinopyroxene-liquid geothermometer is whether clinopyroxene are in equilibrium with coexisting liquid in natural samples. If the mineral did not crystallize in equilibrium with the liquid, results returned by a geothermometer that is based on these two compositions—such as ours—will be suspect. To investigate clinopyroxene-liquid equilibrium and provide a tool for assessing equilibrium in conjunction with our geothermometer, major element partition coefficients were calculated for all experimental compositions in the calibration data set (n = 64), as well as for the larger data set (n = 1290) used to calibrate the Putirka (2008) geothermometer. Using this combined experimental data set, we find SiO_2 clinopyroxene-liquid partition coefficients to be a reliable indicator of equilibrium, with mafic samples having $Kd_{SiO_2}^{Cpx-liquid} > 1.0$ (average = 1.03), rhyolitic samples having $Kd_{SiO_2}^{Cpx-liquid} < 0.75$ (average = 0.68), and intermediate silica samples having intermediate $Kd_{SiO_2}^{Cpx-liquid}$ values (average

= 0.81). Thus, we advise using clinopyroxene-liquid pairs with our geothermometer only when the $Kd_{SiO_2}^{Cpx-liquid}$ is <0.75. The natural samples explored in the discussion section have average $Kd_{SiO_2}^{Cpx-liquid}$ = 0.66, indicating clinopyroxene is in equilibrium with rhyolitic liquids in these systems.

Application to natural systems

Here we use the new geothermometer to calculate temperatures for several natural high-silica systems (Table 4, Supplemental[1] Table S3). In all cases the new geothermometer yields temperatures that are lower than those calculated with the Putirka (2008, Eq. 33) geothermometer; for the Bishop Tuff, Bandelier Tuff, and Paektu comendite, this difference is 130 °C on average (Fig. 4). For all high-silica systems considered, the new geothermometer calculates temperatures that are more consistent with our understanding of those systems, as well as with experimental phase equilibria and other mineral-derived temperatures.

Late-erupted Bishop Tuff, Long Valley

The 0.76 Ma late-erupted Bishop Tuff (Ig2) was emplaced at Long Valley Caldera in eastern California near the end of an eruption whose eruptive products covered as much as 2.5 × 10^6 km^2 of North America (Hildreth and Wilson 2007). The Bishop Tuff has been intensely studied (e.g., Hildreth 1977, 1981; Hervig and Dunbar 1992; Wilson and Hildreth 1997; Anderson et al. 2000; Bindeman and Valley 2002; Reid et al. 2011; Gualda and Ghiorso 2013; Chamberlain et al. 2014; Gualda and Sutton 2016) with particular interest in the possible stratification of the magma body before eruption, a hypothesis based on Fe-Ti oxide geothermometry. Fe-Ti oxide QUILF geothermometry (Anderson et al. 1993) returns a temperature over 800 °C for the late-errupted ignimbrite and a temperature of ~720 °C for the earlier units (Hildreth and Wilson 2007; Ghiorso and Evans 2008). Similarly, quartz-magnetite oxygen isotope geothermometry returns 815 °C for the late-erupted units and 715 °C for the early erupted units (Bindeman and Valley 2002). However, Gardner et al. (2014) and Ghiorso and Gualda (2013) suggest that the Fe-Ti oxides did not crystallize in equilibrium with the rest of the Bishop Tuff phase assemblage and that the oxygen isotope geothermometry may not reflect magmatic storage temperatures. Instead, Gardner et al. (2014) suggest a pre-eruptive storage temperature of <740 °C based on phase equilibria experiments on the late-erupted Bishop Tuff composition.

Pyroxene phenocrysts are not present in the early-erupted Bishop Tuff, but clinopyroxene is present in the late-erupted Bishop Tuff (Table 4, Supplemental[1] Table S3). Experimental studies of late-erupted Bishop Tuff pumice containing 20% phenocrysts of quartz, sanidine, plagioclase, clinopyroxene, orthopyroxene, biotite, magnetite, and ilmenite indicate that clinopyroxene does not crystallize at temperatures above 800 °C at pressures >1.4 kbar and is unlikely to crystallize above 820 °C at pressures ≤1.2 kbar (Pamukcu et al. 2012; Gardner et al. 2014). The Putirka (2008, Eq. 33) clinopyroxene-liquid geothermometer calculates 870 °C for the late-erupted Bishop Tuff natural clinopyroxene rims, which places the clinopyroxene crystallization interval far above the experimental liquidus of Gardner et al. (2014) (Fig. 5). The new geothermometer calculates a late-erupted clinopyroxene temperature of 759 °C that is well within the clinopyroxene's stability field in experimental studies and is also consistent with the Gardner et al. (2014) storage temperature and Ti-in-zircon geothermometry (Gualda and Ghiorso 2013) (Fig. 5). The lower clinopyroxene temperature of 759 °C is also closer to the Fe-Ti oxide and oxygen isotope temperatures for the early erupted units, lending support to the argument that this material may not have

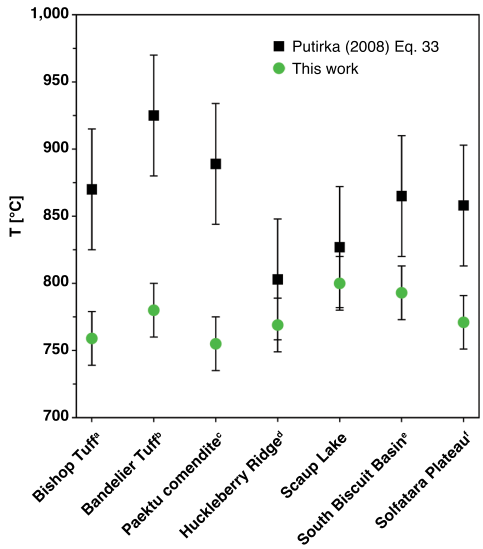

Figure 4. Natural clinopyroxene temperatures calculated with clinopyroxene-liquid geothermometers. Average ΔT is 87 °C. Compositional data from [a] Hildreth (1977) and Gardner et al. (2014), [b] Warshaw and Smith (1988) and Wilcock et al. (2013), [c] Iacovino et al. (2016), [d] Sisson (1991), [e] Girard and Stix (2010), and [f] Befus and Gardner (2016) and Girard and Stix (2010) available in Supplemental[1] Table 3. (Color online.)

Table 4. Average natural clinopyroxene compositions and clinopyroxene-liquid temperatures

Locality	SiO_2	TiO_2	Al_2O_3	Cr_2O_3	FeO^{tot}	MnO	MgO	CaO	Na_2O	K_2O	*T* (°C)
Scaup Lake	51.56	0.17	0.64	0.01	15.42	0.75	11.13	19.97	0.32	0.03	800
	0.26	*0.02*	*0.04*	*0.01*	*0.51*	*0.05*	*0.23*	*0.24*	*0.02*	*0.01*	
South Biscuit Basin[a]	51.81	0.19	0.68	0.00	16.54	0.84	10.76	18.87	0.29	0.02	793
Solfatara Plateau[b]	49.34	0.22	0.48	0.00	26.37	0.87	4.12	18.29	0.30	0.01	771
Bishop Tuff[c]	51.98	0.15	0.74	0.00	12.82	0.57	12.69	20.65	0.38	0.00	759
Paektu Millennium[d]	48.94	0.22	0.20	0.00	28.75	0.88	0.86	18.46	1.70	0.00	755
Lava Creek Tuff A[e]	48.95	0.20	0.64	0.00	25.11	0.71	5.59	18.48	0.32	0.00	805
Lava Creek Tuff B[e]	48.57	0.23	0.62	0.00	26.68	0.73	4.48	18.38	0.31	0.00	776
Huckleberry Ridge Tuff[f]	48.49	0.20	0.60	0.00	27.40	0.86	3.28	18.89	0.30	0.00	769
Bandelier Tuff[g]	52.08	0.14	0.51	0.00	22.19	1.97	7.10	15.46	0.56	0.00	780

Notes: Standard deviation in italics for this work. Oxides given in wt% and normalized. SEE for temperature calculations is ±20 °C. Complete data from [a] Girard and Stix (2010), [b] Girard and Stix (2010) and Befus and Gardner (2016), [c] Hildreth (1977) and Gardner et al. (2014), [d] Iacovino et al. (2016), [e] Hildreth, personal communication, [f] Sisson (1991), and [g] Warshaw and Smith (1988) are available in Supplemental[1] Table S3.

been stored at much higher temperatures than the early erupted products, and thus does not support a vertical stratification model for the Bishop Tuff magma body. Workers have suggested the pyroxene-free early erupted material may have been stored laterally to the late-erupted material (Wilson and Hildreth 1997; Cashman and Giordano 2014), and the new geothermometer results for the Bishop Tuff could lend credence to this hypothesis.

Millennium eruption comendite, Paektu

Paektu (also known as Changbaishan) is a high-silica igneous system located on the border of the Democratic People's Republic of Korea and China. Circa 946 AD, the Paektu Millennium Eruption deposited 23 ± 5 km^3 DRE of tephra, most of which is comendite pumice containing alkali feldspar, clinopyroxene (Table 4, Supplemental[1] Table S3), fayalite, Fe-Ti oxides, and quartz (Horn and Schmincke 2000). Phase equilibria experiments for this system indicate that clinopyroxene is the liquidus phase, with the liquidus at ~720 °C at 1 kbar and ~770 °C at 500 bar (Iacovino et al. 2015, 2016). Similar to the above results for the Bishop Tuff, the Putirka (2008, Eq. 33) clinopyroxene-liquid geothermometer returns a superliquidus temperature of 889 °C for the Millennium Eruption comendite pumice, whereas the new geothermometer yields a temperature of 755 °C, which approximates the temperature experimentally determined to best reproduce the natural phase assemblage (725 °C at 500 bar; Iacovino et al. 2015, 2016). Paektu is yet to be studied in depth, and it remains unclear whether the Millennium Eruption was the caldera-forming eruption. The new clinopyroxene-liquid geothermometer could help elucidate Paektu's history in future investigations.

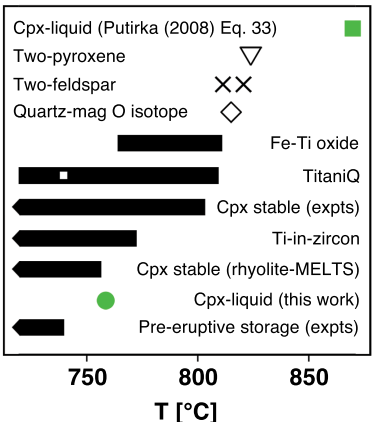

FIGURE 5. Comparison of temperatures and clinopyroxene stability for the late-erupted Bishop Tuff (Ig2). Clinopyroxene-liquid (Putirka 2008, Eq. 33), two-pyroxene (Frost and Lindsley 1992), two-feldspar (Chamberlain et al. 2014), and quartz-magnetite oxygen isotope (Bindeman and Valley 2002) temperatures all are higher than the experimental liquidus/clinopyroxene-in of Gardner et al. (2014). Fe-Ti oxide (Frost and Lindsley 1992) and TitaniQ (Wark et al. 2004, 2007) temperature ranges straddle this liquidus (white square = average TitaniQ temperature). The clinopyroxene-liquid temperature of this work is below the experimental liquidus, experimental liquidus and is more consistent with the rhyolite-MELTS clinopyroxene-in, the Gardner et al. (2014) Bishop Tuff pre-eruptive storage temperature, and the Ti in zircon in zircon temperature (Gualda and Ghiorso 2013) than the Putirka (2008, Eq. 33) clinopyroxene-liquid temperature. (Color online.)

Scaup Lake rhyolite, Yellowstone

High-Fe, low-Al clinopyroxene is the most abundant mafic phase in the Scaup Lake rhyolite, a lava emplaced effusively ca. 257 ka, after the last caldera-forming eruption at Yellowstone (Christiansen et al. 2007; Girard and Stix 2009). Scaup Lake clinopyroxene (Table 4, Supplemental[1] Table S3) exhibit exsolution lamellae, are reverse zoned with higher-Fe cores, and have alternating higher- and lower-Fe fine rim zones, all indicators of a complex pre-eruptive history involving both thermal and chemical variation (Till et al. 2015). The Putirka (2008, Eq. 33) clinopyroxene-liquid geothermometer was unable to calculate temperatures for several Scaup Lake clinopyroxene-liquid pairs because the Scaup Lake clinopyroxene have, on average, Jd < 0.008. The new clinopyroxene-liquid geothermometer yields a temperature of 800 °C for the outermost rim of these clinopyroxene, which is slightly lower than that of the Putirka (2008, Eq. 33) geothermometer (827 °C when able to be calculated) and much lower than the two-pyroxene temperature of ~880 °C obtained via PyMELTS (Sack and Ghiorso 1994) and QUILF. Other post-caldera lavas from Yellowstone, the South Biscuit Basin and Solfatara Plateau rhyolites emplaced ca. 255 and 103 ka, respectively (Christiansen 2001; Bindeman et al. 2008), yield new geothermometer temperatures ~80 °C lower than the temperatures calculated by the Putirka (2008, Eq. 33) clinopyroxene-liquid geothermometer (Fig. 4), underlining the importance of using the new geothermometer for the Yellowstone system.

We judge the new temperature to be the preferred temperature for Scaup Lake clinopyroxene rim growth because, unlike the Putirka (2008, Eq. 33) clinopyroxene-liquid geothermometer, the new geothermometer is able to calculate temperatures for all Scaup Lake clinopyroxene compositions and does not rely on the presence of co-crystallizing orthopyroxene, so it can be used if there is any uncertainty about phase equilibria. This temperature is slightly lower than that recorded by prior Fe-Ti oxide geothermometry (834–880 °C: Hildreth et al. 1984; Vazquez et al. 2009) and two-feldspar geothermometry (819 ± 20 °C: Till et al. 2015), differences we do not interpret as an error in geothermometry but rather as a reflection of the relative location of phase boundaries and a particular mineral-element pair's ability to diffusively re-equilibrate.

For example, Scaup Lake quartz return temperatures of 849 ± 13 °C for cores and 862 ± 10 °C for rims (Vazquez et al. 2009) via TitaniQ (Wark and Watson 2006). The new geothermometer's clinopyroxene rim temperature of 800 °C indicates that clinopyroxene continues to crystallize at or below the temperatures of the quartz-in phase boundary for the Scaup Lake rhyolite. Although there are questions as to the effect of growth rate and a_{TiO_2} on TitaniQ (e.g., Huang and Audétat 2012; Ghiorso and Gualda 2013; Pamukcu et al. 2016), this is the same relative positioning of the quartz-in and clinopyroxene-in phase boundaries observed in experiments on other similar composition systems such as the Blacktail Creek Tuff (Bolte et al. 2015) and Solfatara Plateau rhyolite (Befus and Gardner 2016).

The 800 °C rim crystallization temperature returned by the new geothermometer is also more consistent with our understanding of how exsolution lamellae form parallel to [100] in the cores of clinopyroxene, a feature that is observed in the Scaup Lake clinopyroxene. Experimental studies show that orthopyroxene-in-augite lamellae require temperatures below 825 °C to form (Huebner

1980; Lindsley 1983). Temperatures calculated for Scaup Lake by other methods are too high to account for the formation of the lamellae, e.g., 862 ± 36 °C (Shaffer and Till 2016) via plagioclase-liquid geothermometry (Putirka 2008) and 876 ± 29 °C via QUILF two-pyroxene geothermometry.

Lava Creek Tuff and Huckleberry Ridge Tuff, Yellowstone

The Lava Creek Tuff is the product of the third, and most recent, caldera-forming eruption at Yellowstone that blanketed much of the continental United States in ash ca. 631 ka (Matthews et al. 2015). The Lava Creek Tuff is dominantly composed of two members, LCT-A and LCT-B, which are indistinguishable in age and separated by a layer of fallout ash (Christiansen 2001). High-Fe, low-Al clinopyroxene (Table 4, Supplemental[1] Table S3) were described in both members by Hildreth et al. (1984). The new clinopyroxene-liquid geothermometer calculates temperatures for LCT-A and LCT-B of 805 and 776 °C, respectively. These temperatures correspond within error with geothermometry of other LCT-B phases, sanidine: 814 ± 23 °C via the Putirka (2008) alkali feldspar-liquid geothermometer and quartz: 815 ± 25 °C via TitaniQ (Shamloo and Till 2019), as well as an LCT-B magma storage temperature of 800 ± 50 °C determined using the rhyolite-MELTS geothermometer (Gualda and Ghiorso 2015; Befus et al. 2018). Hildreth (1981) conducted Fe-Ti oxide geothermometry of both members, calculating ~800 °C for LCT-A and ~950 °C for LCT-B, implying a thermal gradient in the magma body similar to that proposed for the Bishop Tuff. However, the new clinopyroxene-liquid temperatures are just within the uncertainty of each other and do not support the interpretation of a thermal gradient. The Putirka (2008, Eq. 33) clinopyroxene-liquid geothermometer does not return temperatures for any of these natural samples, reinforcing the utility of the new geothermometer.

The Putirka (2008, Eq. 33) clinopyroxene-liquid geothermometer does return temperatures for clinopyroxene-liquid pairs from the Huckleberry Ridge Tuff, which was erupted during Yellowstone's first caldera-forming eruption ca. 2.1 Ma (Christiansen 2001), and contains compositionally similar clinopyroxene to that of the Lava Creek Tuff. The new clinopyroxene-liquid geothermometer returns a temperature for Huckleberry Ridge of 769 °C, which is more than 30 °C lower than the Putirka (2008, Eq. 33) geothermometer and below the rhyolite-MELTS-calculated liquidus for this system when modeled at 4.7 wt% H_2O (Gualda et al. 2012; Myers et al. 2016). A clinopyroxene-liquid temperature of 769 °C is also consistent with two-feldspar geothermometry for the ignimbrite of 768–855 °C (Elkins and Grove 1990; Swallow et al. 2018). The new clinopyroxene-liquid temperatures for these large siliceous tuffs ≤805 °C implies that these minerals were last crystallizing at near-solidus conditions and at relatively high crystal/liquid ratios.

Implications

In general, the new clinopyroxene-liquid geothermometer lowers calculated temperatures for a given sample by an average of almost 90 °C relative to prior clinopyroxene-liquid geothermometers (Fig. 4). In all cases where experiments are available, the temperature returned by the new geothermometer is between the solidus and liquidus for the relevant bulk composition, indicating that the new clinopyroxene-liquid geothermometer is a better approximation of the relevant geologic conditions than the Putirka (2008, Eq. 33) geothermometer, which consistently returns temperatures above the experimental liquidi or the clinopyroxene-in phase boundaries of silicic magmas. Thus, the new geothermometer reconciles many inconsistencies in previous thermometric results.

It is important to note that clinopyroxene chemistry and stability in high-silica systems is not the same as in mafic systems. Dry experiments on mafic bulk compositions reveal that clinopyroxene is stable from ~1180–1470 °C at 1 atm to 25 kbar and is usually stable in these experiments to at least 25 °C below its first appearance (e.g., Elthon and Scarfe 1984; Grove and Juster 1989; Juster et al. 1989; Bartels et al. 1991; Grove et al. 1992; Kinzler and Grove 1992; Feig et al. 2010, 2006), however experiments on silicic bulk compositions that constrain clinopyroxene stability are exclusively hydrous and restrict clinopyroxene stability to below 1000 °C (e.g., Almeev et al. 2012; Gardner et al. 2014; Bolte et al. 2015; Iacovino et al. 2015). In dry mafic systems above 11 kbar, clinopyroxene is rarely a liquidus phase and may become unstable 25–40 °C after its first appearance (e.g., Elthon and Scarfe 1984; Grove and Juster 1989; Juster et al. 1989; Bartels et al. 1991; Grove et al. 1992; Kinzler and Grove 1992; Feig et al. 2010, 2006). Conversely, in high-silica systems, experiments often place clinopyroxene on the liquidus (Almeev et al. 2012; Gardner et al. 2014; Bolte et al. 2015; Iacovino et al. 2015). And although clinopyroxene is a mafic phase, experiments and our temperature calculations demonstrate that its stability is not restricted to near-liquidus temperatures. We have calculated clinopyroxene in high-silica natural systems to below 775 °C for the late-erupted Bishop Tuff, Paektu comendite, and Bandelier Tuff (Fig. 4, Table 4), and experiments have shown the mineral to crystallize at, or near, the solidus to temperatures as low as 675 °C (e.g., Almeev et al. 2012; Gardner et al. 2014; Bolte et al. 2015; Iacovino et al. 2015; Befus and Gardner 2016). If clinopyroxene stability extends from the liquidus to the solidus in high-silica magma, the presence of clinopyroxene does not necessitate the invocation of xenocrysts, mixing with a hotter magma body, nor imply a low (or high) crystallinity. Instead, clinopyroxene, when present, appears to be a persistent phase throughout the crystallization interval of high-silica systems.

Because of the lack of relevant experiments in its calibration data set, thermodynamic phase equilibria modeling of clinopyroxene-bearing systems using rhyolite-MELTS remains problematic. Although rhyolite-MELTS produces a realistic clinopyroxene crystallization interval—that is, one consistent with the new geothermometer's temperature—for the Bishop Tuff (Fig. 5), it should be noted that rhyolite-MELTS was calibrated for this particular locality and the model does not perform as well for other high-silica systems. Rhyolite-MELTS modeling often places clinopyroxene in the middle of, or late in, the high-silica system crystallization sequence, rather than on the liquidus as suggested by experiments (e.g., Almeev et al. 2012; Gardner et al. 2014; Iacovino et al. 2015). Rhyolite-MELTS failed to predict crystallization of clinopyroxene for 70% of the systems examined for this work, all of which contain clinopyroxene in the equilibrium mineral assemblage. For the trials in which clinopyroxene was predicted (not including the Bishop Tuff), on

average rhyolite-MELTS predicted the clinopyroxene-in phase boundary over 120 °C below the temperatures returned by the new clinopyroxene-liquid geothermometer and experimental phase equilibria, where available. We join other workers in urging caution when using rhyolite-MELTS to simulate systems in which clinopyroxene is present (e.g., Gardner et al. 2014), as its failure to accurately simulate the mineral's behavior may give the mistaken impression that clinopyroxene has a much narrower crystallization interval than in reality, as well as suggest an inaccurate degree of crystallinity.

Finding low-Al clinopyroxene in a lava may be evaluative in and of itself. In high-silica systems, clinopyroxene contains <2 wt% Al_2O_3 (Fig. 1), while it is possible for mafic clinopyroxene to contain >10 wt% Al_2O_3, when compositions are queried from the GEOROC database. The low Al content in rhyolitic clinopyroxene is a result of a need for more Si in tetrahedral sites to compensate for the charge imbalance with O_3 oxygen atoms produced by low Ca content in the crystal (CaO can be <17 wt% in rhyolitic clinopyroxene and up to >23 wt% in basaltic clinopyroxene; data from GEOROC) (Salviulo et al. 2000). Thus, the presence of low-Al clinopyroxene outside of a rhyolite may indicate that the mineral has been inherited from a higher-silica magma or country rock.

Low-Al, high-Fe clinopyroxene may also hint at the thermal history of the lava. Clinopyroxene high in Al have been linked to fast crystal growth and thus high undercooling; during this process the crystal grows faster than the melt can deliver nutrients to the growth surface, causing a depletion of compatible elements in the surrounding melt as well as an enrichment in incompatible elements. As the crystal grows, it incorporates more incompatible elements into its structure, causing an increase in these elements rim-ward (Lofgren et al. 2006; Zhang 2008; Mollo and Hammer 2017). Conversely, crystal rims low in incompatible and high in compatible elements as described herein counterindicate interface-controlled growth and instead imply diffusion-controlled growth wherein the diffusive velocity of elements in the melt is sufficient to deliver the ideal nutrients to the crystal. Additionally, experimental studies on basaltic compositions have correlated low Al with slow cooling rates (e.g., Mollo et al. 2010). The above suggests a slow growth rate for the low-Al, high-Fe clinopyroxene found in high-silica magmatic systems, relative to high-Al clinopyroxene (Zhang 2008). This, combined with our new geothermometer and clinopyroxene's broad stability in high-silica magmatic systems, makes the mineral an attractive tool for investigating a range of processes in these hazardous geological settings.

Funding

This work was supported by the National Park Services research permit YELL-2015-SCI-6078 and by the U.S. National Science Foundation under Graduate Research Fellowship no. 026257-001 to K.K.B. and CAREER EAR-1654584 to C.B.T. The EPMA facilities at ASU are in part supported by the National Nanotechnology Coordinated Infrastructure grant ECCS-1542160. Thank you to Julia Hammer and David Neave whose reviews helped to improve this manuscript.

Acknowledgments

Special thanks to Tim Grove for the use of the experimental petrology lab at MIT, and to Wes Hildreth for sharing his unpublished probe data. Additional thanks to Axel Wittmann, Kayla Iacovino, Jessica Noviello, Crystylynda Fudge, and the EPIC group at ASU. Great appreciation to Keith Putirka whose thoughtful questions and insights have helped guide this research.

References cited

Almeev, R.R., Bolte, T., Nash, B.P., Holtz, F., Erdmann, M., and Cathey, H.E. (2012) High-temperature, low-H_2O silicic magmas of the Yellowstone Hotspot: an experimental study of rhyolite from the Bruneau-Jarbidge Eruptive Center, Central Snake River Plain, USA. Journal of Petrology, 53, 1837–1866.

Anderson, A.T., Davis, A.M., and Lu, F. (2000) Evolution of Bishop Tuff rhyolitic magma based on melt and magnetite inclusions and zoned phenocrysts. Journal of Petrology, 41, 449–473.

Anderson, D.J., Lindsley, D.H., and Davidson, P.M. (1993) QUILF: A pascal program to assess equilibria among Fe, Mg, Mn, Ti oxides, pyroxenes, olivine, and quartz. Computers & Geosciences, 19, 1333–1350.

Bartels, K.S., Kinzler, R.J., and Grove, T.L. (1991) High pressure phase relations of primitive high-alumina basalts from Medicine Lake volcano, northern California. Contributions to Mineralogy and Petrology, 108, 253–270.

Befus, K.S., and Gardner, J.E. (2016) Magma storage and evolution of the most recent effusive and explosive eruptions from Yellowstone Caldera. Contributions to Mineralogy and Petrology, 171, 30.

Befus, K.S., Bruyere, R.H., and Manga, M. (2018) Lava Creek Tuff Love. Presented at the Goldschmidt, Boston, U.S.A.

Bindeman, I.N., and Valley, J.W. (2002) Oxygen isotope study of the Long Valley magma system, California: Isotope thermometry and convection in large silicic magma bodies. Contributions to Mineralogy and Petrology, 144, 185–205.

Bindeman, I.N., Fu, B., Kita, N.T., and Valley, J.W. (2008) Origin and evolution of silicic magmatism at yellowstone based on ion microprobe analysis of isotopically zoned zircons. Journal of Petrology, 49, 163–193.

Bolte, T., Holtz, F., Almeev, R., and Nash, B. (2015) The Blacktail Creek Tuff: an analytical and experimental study of rhyolites from the Heise volcanic field, Yellowstone hotspot system. Contributions to Mineralogy and Petrology, 169, 15.

Cashman, K.V., and Giordano, G. (2014) Calderas and magma reservoirs. Journal of Volcanology and Geothermal Research, 288, 28–45.

Chamberlain, K.J., Morgan, D.J., and Wilson, C.J.N. (2014) Timescales of mixing and mobilisation in the Bishop Tuff magma body: perspectives from diffusion chronometry. Contributions to Mineralogy and Petrology, 168, 1034.

Christiansen, R.L. (2001) The Quaternary and Pliocene Yellowstone Plateau volcanic field of Wyoming, Idaho, and Montana, 145 p. U.S. Geological Survey, Reston, Virginia.

Christiansen, R.L., Lowenstern, J.B., Smith, R.B., Heasler, H., Morgan, L.A., Nathenson, M., Mastin, L.G., Muffler, L.J.P., and Robinson, J.E. (2007) Preliminary Assessment of Volcanic and Hydrothermal Hazards in Yellowstone National Park and Vicinity, p. 94. U.S. Geological Survey.

Elkins, L.T., and Grove, T.L. (1990) Ternary feldspar experiments and thermodynamic models. American Mineralogist, 75, 544–559.

Elthon, D., and Scarfe, C.M. (1984) High-pressure phase equilibria of a high-magnesian basalt and the genesis of primary oceanic basalts. American Mineralogist, 69, 1–15.

Feig, S.T., Koepke, J., and Snow, J.E. (2006) Effect of water on tholeiitic basalt phase equilibria: an experimental study under oxidizing conditions. Contributions to Mineralogy and Petrology, 152, 611–638.

——— (2010) Effect of oxygen fugacity and water on phase equilibria of a hydrous tholeiitic basalt. Contributions to Mineralogy and Petrology, 160, 551–568.

Frost, B.R., and Lindsley, D.H. (1992) Equilibria among Fe-Ti oxides, pyroxenes, olivine, and quartz: Part II. Application. American Mineralogist, 77, 1004–1020.

Gardner, J.E., Befus, K.S., Gualda, G.A.R., and Ghiorso, M.S. (2014) Experimental constraints on rhyolite-MELTS and the Late Bishop Tuff magma body. Contributions to Mineralogy and Petrology, 168, 1051.

Ghiorso, M.S., and Evans, B.W. (2008) Thermodynamics of rhombohedral oxide solid solutions and a revision of the Fe-Ti two-oxide geothermometer and oxygen-barometer. American Journal of Science, 308, 957–1039.

Ghiorso, M.S., and Gualda, G.A.R. (2013) A method for estimating the activity of titania in magmatic liquids from the compositions of coexisting rhombohedral and cubic iron–titanium oxides. Contributions to Mineralogy and Petrology, 165, 73–81.

Girard, G., and Stix, J. (2009) Magma recharge and crystal mush rejuvenation associated with early post-collapse Upper Basin Member Rhyolites, Yellowstone Caldera, Wyoming. Journal of Petrology, 50, 2095–2125.

——— (2010) Rapid extraction of discrete magma batches from a large differentiating magma chamber: the Central Plateau Member rhyolites, Yellowstone Caldera, Wyoming. Contributions to Mineralogy and Petrology, 160, 441–465.

Grove, T.L., and Juster, T.C. (1989) Experimental investigations of low-Ca pyroxene stability and olivine-pyroxene-liquid equilibria at 1-atm in natural basaltic and andesitic liquids. Contributions to Mineralogy and Petrology, 103, 287–305.

Grove, T.L., Kinzler, R.J., and Bryan, W.B. (1992) Fractionation of mid-ocean ridge basalt (MORB). Geophysical Monograph, 71, 281–310.

Gualda, G.A.R., and Ghiorso, M.S. (2013) The Bishop Tuff giant magma body: an alternative to the Standard Model. Contributions to Mineralogy and Petrology, 166, 755–775.

——— (2015) MELTS_Excel: A Microsoft Excel-based MELTS interface for research and teaching of magma properties and evolution. Geochemistry, Geophysics, Geosystems, 16, 315–324.

Gualda, G.A.R., and Sutton, S.R. (2016) The year leading to a supereruption. PLOS One, 11, e0159200.

Gualda, G.A.R., Ghiorso, M.S., Lemons, R.V., and Carley, T.L. (2012) Rhyolite-MELTS: a modified calibration of MELTS optimized for silica-rich, fluid-bearing magmatic

systems. Journal of Petrology, 53, 875–890.
Hervig, R.L., and Dunbar, N.W. (1992) Cause of chemical zoning in the Bishop (California) and Bandelier (New Mexico) magma chambers. Earth and Planetary Science Letters, 111, 97–108.
Hildreth, E.W. (1977) The magma chamber of the Bishop Tuff: Gradients in temperature, pressure, and composition. Ph.D. thesis, University of California, Berkeley.
Hildreth, W. (1981) Gradients in silicic magma chambers: Implications for lithospheric magmatism. Journal of Geophysical Research: Solid Earth, 86, 10153–10192.
Hildreth, W., and Wilson, C.J.N. (2007) Compositional zoning of the Bishop Tuff. Journal of Petrology, 48, 951–999.
Hildreth, W., Christiansen, R.L., and O'Neil, J.R. (1984) Catastrophic isotopic modification of rhyolitic magma at times of caldera subsidence, Yellowstone Plateau Volcanic Field. Journal of Geophysical Research: Solid Earth, 89, 8339–8369.
Horn, S., and Schmincke, H.-U. (2000) Volatile emission during the eruption of Baitoushan Volcano (China/North Korea) ca. 969 AD. Bulletin of Volcanology, 61, 0537–0555.
Huang, R., and Audétat, A. (2012) The titanium-in-quartz (TitaniQ) thermobarometer: A critical examination and re-calibration. Geochimica et Cosmochimica Acta, 84, 75–89.
Huebner, J.S. (1980) Pyroxene phase equilibria at low pressure. Reviews in Mineralogy, 7, 213–288.
Iacovino, K., Kim, J.S., Sisson, T.W., Lowenstern, J.B., Jang, J.N., Song, K.H., Ham, H.H., Ri, K.H., Donovan, A.R., Oppenheimer, C., and others. (2015) New Constraints on the Geochemistry of the Millennium Eruption of Mount Paektu (Changbaishan), Democratic People's Republic of Korea/China. In 2015 AGU Fall Meeting. San Francisco, U.S.A.
Iacovino, K., Kim, J.-S., Sisson, T., Lowenstern, J., Ri, K.-H., Jang, J.-N., Song, K.-H., Ham, S.-H., Oppenheimer, C., Hammond, J.O.S., and others. (2016) Quantifying gas emissions from the "Millennium Eruption" of Paektu volcano Democratic People's Republic of Korea/China. Science Advances, 2, 1–11.
Juster, T.C., Grove, T.L., and Perfit, M.R. (1989) Experimental constraints on the generation of FeTi basalts, andesites, and rhyodacites at the Galapagos Spreading Center, 85°W and 95°W. Journal of Geophysical Research, 94, 9251.
Kinzler, R.J., and Grove, T.L. (1992) Primary magmas of mid-ocean ridge basalts 1. Experiments and methods. Journal of Geophysical Research, 97, 6885.
Liang, Y., Sun, C., and Yao, L. (2013) A REE-in-two-pyroxene thermometer for mafic and ultramafic rocks. Geochimica et Cosmochimica Acta, 102, 246–260.
Lindsley, D.H. (1983) Pyroxene thermometry. American Mineralogist, 68, 477–493.
Lindsley, D.H., and Andersen, D.J. (1983) A two-pyroxene thermometer. Journal of Geophysical Research, 88, A887.
Lofgren, G.E., Huss, G.R., and Wasserburg, G.J. (2006) An experimental study of trace-element partitioning between Ti-Al-clinopyroxene and melt: Equilibrium and kinetic effects including sector zoning. American Mineralogist, 91, 1596–1606.
Masotta, M., Mollo, S., Freda, C., Gaeta, M., and Moore, G. (2013) Clinopyroxene–liquid thermometers and barometers specific to alkaline differentiated magmas. Contributions to Mineralogy and Petrology, 166, 1545–1561.
Matthews, N.E., Vazquez, J.A., and Calvert, A.T. (2015) Age of the Lava Creek supereruption and magma chamber assembly from combined $^{40}Ar/^{39}Ar$ and U-Pb dating of sanidine and zircon crystals. Geochemistry, Geophysics, Geosystems, 16, 2508–2528, doi: 10.1002/2015GC005881.
Mollo, S., and Hammer, J.E. (2017) Dynamic crystallization in magmas. In W. Heinrich and R. Abart, Eds., Mineral Reaction Kinetics: Microstructures, Textures, Chemical and Isotopic Signatures, vol. 16, p. 378–418. Mineralogical Society of Great Britain & Ireland.
Mollo, S., Del Gaudio, P., Ventura, G., Iezzi, G., and Scarlato, P. (2010) Dependence of clinopyroxene composition on cooling rate in basaltic magmas: Implications for thermobarometry. Lithos, 118, 302–312.
Myers, M.L., Wallace, P.J., Wilson, C.J.N., Morter, B.K., and Swallow, E.J. (2016) Prolonged ascent and episodic venting of discrete magma batches at the onset of the Huckleberry Ridge supereruption, Yellowstone. Earth and Planetary Science Letters, 451, 285–297.
Pamukcu, A.S., Gualda, G.A.R., and Anderson, A.T. (2012) Crystallization stages of the Bishop Tuff magma body recorded in crystal textures in pumice clasts. Journal of Petrology, 53, 589–609.
Pamukcu, A.S., Ghiorso, M.S., and Gualda, G.A.R. (2016) High-Ti, bright-CL rims in volcanic quartz: a result of very rapid growth. Contributions to Mineralogy and Petrology, 171, 105.
Putirka, K.D. (2008) Thermometers and barometers for volcanic systems. Reviews in Mineralogy and Geochemistry, 69, 61–120.
Putirka, K.D., Mikaelian, H., Ryerson, F., and Shaw, H. (2003) New clinopyroxene-liquid thermobarometers for mafic, evolved, and volatile-bearing lava compositions, with applications to lavas from Tibet and the Snake River Plain, Idaho. American Mineralogist, 88, 1542–1554.
Reid, M.R., Vazquez, J.A., and Schmitt, A.K. (2011) Zircon-scale insights into the history of a Supervolcano, Bishop Tuff, Long Valley, California, with implications for the Ti-in-zircon geothermometer. Contributions to Mineralogy and Petrology, 161, 293–311.
Sack, R.O., and Ghiorso, M.S. (1994) Thermodynamics of multicomponent pyroxenes: II. Phase relations in the quadrilateral. Contributions to Mineralogy and Petrology, 116, 287–300.
Salviulo, G., Secco, L., Marzoli, A., Piccirillo, E.M., and Nyobe, J.B. (2000) Ca-rich pyroxene from basic and silicic volcanic rocks from the Cameroon Volcanic Line (West-Africa): crystal chemistry and petrological relationships. Mineralogy and Petrology, 70, 73–88.
Shaffer, J.S., and Till, C.B. (2016) New temperature and H_2O estimates for Post Caldera Yellowstone Rhyolite Lavas using feldspar geothermometry and rhyolite-MELTS. In 2016 AGU Fall Meeting. San Francisco, U.S.A.
Shamloo, H.I., and Till, C.B. (2019) Decadal transition from quiescence to supereruption: petrologic investigation of the Lava Creek Tuff, Yellowstone Caldera, WY. Contributions to Mineralogy and Petrology, 174, 32.
Sisson, T.W. (1991) Pyroxene-high silica rhyolite trace element partition coefficients measured by ion microprobe. Geochimica et Cosmochimica Acta, 55, 1575–1585.
Swallow, E.J., Wilson, C.J.N., Myers, M.L., Wallace, P.J., Collins, K.S., and Smith, E.G.C. (2018) Evacuation of multiple magma bodies and the onset of caldera collapse in a supereruption, captured in glass and mineral compositions. Contributions to Mineralogy and Petrology, 173, 33.
Till, C.B., Vazquez, J.A., and Boyce, J.W. (2015) Months between rejuvenation and volcanic eruption at Yellowstone caldera, Wyoming. Geology, 43, 695–698.
Vazquez, J.A., Kyriazis, S.F., Reid, M.R., Sehler, R.C., and Ramos, F.C. (2009) Thermochemical evolution of young rhyolites at Yellowstone: Evidence for a cooling but periodically replenished postcaldera magma reservoir. Journal of Volcanology and Geothermal Research, 188, 186–196.
Wark, D.A., and Watson, E.B. (2006) TitaniQ: a titanium-in-quartz geothermometer. Contributions to Mineralogy and Petrology, 152, 743–754.
Wark, D.A., Hildreth, W., Watson, E.B., and Cherniak, D.J. (2004) Origin of thermal and compositional zoning in the Bishop Magma Reservoir: Insights from zoned quartz phenocrysts p. 3. Presented at the 2004 AGU Fall Meeting, San Francisco, California, U.S.A.
Wark, D.A., Hildreth, W., Spear, F.S., Cherniak, D.J., and Watson, E.B. (2007) Pre-eruption recharge of the Bishop magma system. Geology, 35, 235.
Warshaw, C.M., and Smith, R.L. (1988) Pyroxenes and fayalites in the Bandelier Tuff, New Mexico: temperatures and comparison with other rhyolites. American Mineralogist, 73, 1025–1037.
Wilcock, J., Goff, F., Minarik, W.G., and Stix, J. (2013) Magmatic recharge during the formation and resurgence of the Valles Caldera, New Mexico, USA: Evidence from quartz compositional zoning and geothermometry. Journal of Petrology, 54, 635–664.
Wilson, C.J.N., and Hildreth, W. (1997) The Bishop Tuff: New insights from eruptive stratigraphy. The Journal of Geology, 105, 407–440.
Zhang, Y. (2008) Geochemical Kinetics, 631 p. Princeton University Press, New Jersey.

Manuscript received October 8, 2018
Manuscript accepted March 28, 2019
Manuscript handled by Charles Lesher

Endnote:

[1]Deposit item AM-19-76842, Supplemental Material. Deposit items are free to all readers and found on the MSA website, via the specific issue's Table of Contents (go to http://www.minsocam.org/MSA/AmMin/TOC/2019/Jul2019_data/Jul2019_data.html).